RSC Advances

PAPER

Published on 24 July 2026

Cite this: DOI: 10.1039/d6ra04478f

The pressure effect on the crystal structure and vibration spectra of the brownmillerite Ca_2FeCoO_5 compound

L. H. Khiem,[ab] S. E. Kichanov,[c] O. N. Lis,[c] E. V. Lukin,[c] N. T. Nguyen,[cde] N. O. Golosova,[c] A. G. Asadov,[c] T. P. Hoang,[fg] Truong-Tho Nguyen,[d] N. V. Tien,[h] L. T. P. Thao[i] and N. T. Dang *[fg]

Pressure-induced phase transitions in complex perovskite materials can significantly alter their physical properties. The discovery of new types of these transitions is important not only for fundamental research, but also for potential practical applications. The structural and vibrational properties of the brownmillerite compound Ca_2FeCoO_5, synthesized using the sol–gel method, have been studied using X-ray diffraction and Raman spectroscopy at pressures up to 24 GPa. A gradual structural transition was observed at pressures above ~6 GPa, evidenced by changes in lattice parameters, unit cell compressibility, and anomalies in vibration mode pressure behaviors. The lattice parameters, unit cell volumes and vibration modes as functions of pressure for the initial orthorhombic phase and the pressure induced phase of brownmillerite Ca_2FeCoO_5 compound were obtained. It is assumed that the observed phase transition is attributed to the reorientation and rearrangement of $Fe(Co)O_4$ tetrahedra and the enhanced distortion of oxygen octahedra $Fe(Co)O_6$. It is also confirmed by the anomalies in the pressure behavior of Raman modes associated with the stretching and bending vibrations of the tetrahedral and octahedral oxygen units.

Received 22nd May 2026
Accepted 21st July 2026

DOI: 10.1039/d6ra04478f

rsc.li/rsc-advances

1. Introduction

Interest in the study of complex perovskite oxides continues to this day, primarily due to their wide range of intriguing and unique physical properties.[1,2] These include electronic and ionic conductivity,[2,3] piezoelectricity, superconductivity, ferroelectricity,[3,4] magnetism,[5,6] and multiferroicity.[7] The complex structural features of these oxides give rise to interesting magnetic phenomena,[5–7] including ferrimagnetism, antiferromagnetism, canted magnetic ordering, spin-glass, and spin-liquid states. This unique set of magnetic properties makes perovskite oxides valuable for a variety of technological applications,[1,4,8] such as biomaterials, smart drug delivery systems, solid oxide fuel cells, batteries, magnetic data storage, magnetic refrigeration, catalysis, and more.

The perovskite-type oxides of transition metals with unconventional oxidation states or complex structural features provide a novel perspective on materials with potential applications in spintronics or electronics. One of them is $Ca_3Co_2O_6$,[9–15] which is an excellent example of a low-dimensional magnetic material that exhibits the spin density wave magnetic state.[9,10,12] The use of colloidal chemical approaches in the preparation of doped $Ca_3Co_2O_6$ materials has special advantages.[16–18] In particular, the co-precipitation of reagents from a solution allows for varying the synthesis conditions over a wide range and controlling the composition, structure, particle morphology, and magnetic properties of the final product by creating metastable phases with a high concentration of defects.[19–21] On the other hand, a high concentration of oxygen vacancies and their structure ordering can cause the formation of new structural types of $Ca_2Co_2O_5$-related compounds.[22,23] So, the formation of the $Ca_2Co_2O_5$ phase during the synthesis of $Ca_3Co_2O_6$ by the sol–gel method is realized.[18,24–27] At the initial stage, precursor salts, such as nitrates or acetates of calcium and cobalt, are dissolved in an

[a]Institute of Physics, Vietnam Academy of Science and Technology, 100000 Hanoi, Vietnam
[b]Dzhelepov Laboratory of Nuclear Problems, Joint Institute of Nuclear Research, Dubna, 141980, Russia
[c]Frank Laboratory of Neutron Physics, Joint Institute for Nuclear Research, 141980 Dubna, Russia
[d]Faculty of Electronics, Electrical Engineering and Material Technology, University of Sciences, Hue University, 530000 Hue, Vietnam
[e]Institute of Oceanography, Vietnam Academy of Science and Technology, Nha Trang 650000, Vietnam
[f]Institute of Research and Development, Duy Tan University, 550000 Danang, Vietnam. E-mail: dangtoan2107@gmail.com; dangngoctoan1@duytan.edu.vn
[g]Faculty of Environmental and Natural Sciences, Duy Tan University, 550000 Danang, Vietnam
[h]Ho Chi Minh City University of Technology and Engineering, Ho Chi Minh City 70000, Vietnam
[i]The University of Danang – University of Science and Education, 550000 Danang, Vietnam

organic solvent, often with the addition of citric acid and ethylene glycol. The citric acid acts as a chelating agent, forming stable complexes with cations such as Ca^{2+} and Co^{2+}/Co^{3+}. When the solution evaporates, a polymer gel forms, in which the cations become trapped in a network of organic ligands.[17,18,26] However, it does not ensure thermodynamic stability for all possible phases under subsequent heating or other processing conditions.[24,26–28] In addition, sol–gel synthesis is accompanied by the formation of a high concentration of structural defects, such as oxygen vacancies, antisites, and cationic disorder clusters.[29] These are favorable for the formation of metastable phases, specifically $Ca_2Co_2O_5$ or Ca_2CoFeO_5,[30] which have a structure similar to that of brownmillerite-type phases. These phases have excessive free energy, which contributes to the formation of not only the target phase but also other phases. In brownmillerite structures, alternating layers with tetrahedral and octahedral cation coordination (Fig. 1) determine the anisotropy of structural and corresponding physical properties.

Regarding anion-deficient metastable phases with structural vacancy ordering,[30–32] research at high pressures is essential for the vacancy-rich brownmillerite phase.[33–36] It is precisely high pressures used as a method to control the change in interatomic distances and related physical properties that can reveal the stability of a particular crystal structure under high pressure.[37,38] The defective structure, primarily due to the presence of ordered oxygen vacancies in the $Ca_2Co_2O_5$ brownmillerite phase,[30] actively redefines how the crystal structure and related physical properties react to high pressure. High pressure can trigger the movement of vacancies or alter their order, resulting in an unexpected phase transition. This can lead to a reorganization of the coordination environment, including changes in the angles between polyhedral units, shifts in cation positions, and the formation of new paths for ion movement. The structure of defects can stabilize a certain phase by creating specific arrangements of vacancies. It can also create energy barriers that prevent transitions to other phases. In addition, the pressure-dependent lattice parameters and vibration spectra can also be used to obtain important thermodynamic parameters, such as the bulk modulus and Grüneisen parameter, which are essential for first-principles calculations. So, the primary high-pressure measurements indicate that the compressibility of brownmillerite-type $Ca_2Fe_2O_5$ (ref. 33 and 34) is significantly lower than that of $CaSiO_3$ perovskite. This suggests an elastic softening due to oxygen vacancies. Also, the result of the high-pressure Raman spectroscopic study[34,36] showed that a phase transition occurred in srebrodolskite $Ca_2Fe_2O_5$ at a pressure of $P \sim 12$ GPa. When similar structural phase transition occurs in Ca_2FeAlO_5,[35] a small jump of the $(Fe,Al)O_4$ tetrahedral bond lengths is observed, which induces a slight jump in lattice parameters.

In our work, we synthesized the brownmillerite phase of Ca_2FeCoO_5 using the colloidal method. The effect of high pressure on this compound has not been investigated. To obtain information about the pressure dependence of the crystal structure and vibrational spectra of the synthesized Ca_2FeCoO_5 compound, we prepared experiments using X-ray and Raman spectroscopy at high pressures up to 25 GPa.

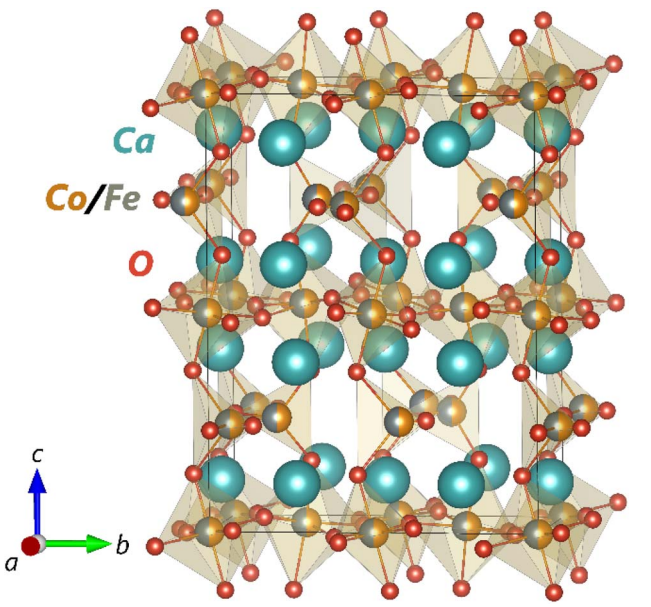

Fig. 1 The schematic representation of the cubic crystal structure of $Ca_2Co_2O_5$ brownmillerite phase at ambient conditions. Fe and Co atoms are mixed and sit in the (4d) position of the tetrahedral site, in (4a) and (4c) positions of the octahedral sites.[30]

2. Experimental

In this study, the brownmillerite-type Ca_2FeCoO_5 material was synthesized *via* a citric acid-assisted sol–gel route.[18,39] This colloidal "soft chemistry" approach was specifically chosen to ensure atomic-level mixing of the constituent metal cations and to deliberately induce a high concentration of structural oxygen vacancies in the final lattice. Stoichiometric amounts of $Ca(NO_3)_2 \cdot 4H_2O$, $Co(NO_3)_2 \cdot 6H_2O$, and $Fe(NO_3)_3 \cdot 9H_2O$ (corresponding to a molar ratio of $Ca : Fe : Co = 2 : 1 : 1$) were dissolved in 10 mL of distilled water. Citric acid, acting as a multidentate chelating agent, was weighed and added to the solution. The mixture was magnetically stirred for 30 min to facilitate complete coordination between the carboxylate and hydroxyl groups of the citric acid and the dissolved metal cations. This crucial chelation step prevents the premature phase separation or precipitation of individual metal oxides, ensuring a highly homogeneous distribution of metal ions within the precursor matrix.

Upon heating the solution in a thermostatic bath at 80 °C, the continuous evaporation of water and subsequent thermal polycondensation reactions led to the formation of a viscous, three-dimensional polymeric gel network. The resulting gel was dried at 200 °C for 7 h to obtain a porous xerogel, where the coordinated metal ions remain firmly trapped within the cross-linked organic matrix. The sample was ground using an agate mortar to enhance fineness and homogeneity, then transferred to a crucible. Finally, the thermal decomposition of this organic–inorganic network during calcination in a furnace at

1000 °C for 10 h (with a heating rate of 200 °C h^{-1}) drove the structural crystallization of the mixed-metal oxide. The vigorous outgassing and evolution of gaseous by-products (CO_x, NO_x, H_2O) during the combustion of the organic framework directly contributes to the stabilization of the metastable, anion-deficient brownmillerite structure. This synthesis regime creates a highly defective oxygen sublattice, inherently defining the alternating octahedral (CoO_6/FeO_6) and tetrahedral (FeO_4/CoO_4) coordination geometries characteristic of the Ca_2FeCoO_5 phase. The resulting dark brown powder was quantitatively harvested, finely pulverized, and stored under vacuum conditions to prevent any atmospheric moisture reabsorption or carbonation before advanced tests. The synthesized sample was characterized by X-ray photoelectron spectroscopy.[40] Table S1 and Fig. S1 of the SI show the binding energies of the peaks corresponding to the constituent elements in the Ca_2FeCoO_5 compound. The values obtained are in good agreement with previously reported data.[41–43] The XPS results indicate that cobalt ions coexist as high-spin Co^{2+} and low-spin state Co^{3+} states,[41] while Fe^{3+} ions occupy both tetrahedral and octahedral sites in the crystal structure of Ca_2CoFeO_5.[42,43] The O 1s spectrum is characterized by two peaks located at 529.44 and 531.51 eV (Fig. S1d), which can be attributed to lattice oxygen (O_L) and adsorbed oxygen-containing surface species (O_{ad}), respectively.[44,45]

In the *in situ* high-pressure experiments, a Boehler–Almax diamond anvil cell (DAC) was employed to achieve high pressures of up to 25.5 GPa. The diamonds had culets of 300 μm in diameter. The sample was inserted into a hole with diameter of 150 μm in a rhenium gasket, which was indented to a depth of approximately 30 μm. The pressure was measured using the ruby fluorescence technique[46] with three ruby spheres: one in the center of the gasket and two near the edges. The accuracy of pressure measurement at each ruby was within 0.1 GPa.

The X-ray diffraction (XRD) experiments were performed using the SAXS/WAXS XEUSS 3.0 system (produced by Xenocs SAS, Grenoble, France) and operated at FLNP JINR (Dubna, Russia), with the Dectris Eiger 2R 500K detector. The wavelength of Mo Kα radiation was $\lambda = 0.7115$ Å. The XRD data were analyzed using the software package FullProf.[47]

The high-pressure measurements were performed without a pressure-transmitting medium due the existence of a glass transition in the 4 : 1 methanol–ethanol mixture is observed at ~10–12 GPa and creates a non-hydrostatic environment rendering it ineffective at the higher pressures probed in present study. No pressure-transmitting medium was employed to prevent its interaction with the sample, thereby enhancing the background conditions for Raman spectroscopy experiments.

Raman spectra at high pressures and ambient temperature were obtained using a Confotec MR200 spectrometer (produced by SOL Instruments GmbH, Augsburg, Germany and operated at FLNP JINR in Dubna, Russia) with a wavelength excitation of 532 nm from a diode-pumped solid-state laser, 1800 mm grating, a confocal hole of 100 μm, and a ×20 objective. The laser power was 17 mW. An absorption coefficient of the studied material for laser excitation wavelengths in the range 488–633 nm is relatively low, and the local heating effects should be negligible. The absence of noticeable laser heating is confirmed by the constant positions of the main Raman modes across the entire laser power range (see Fig. S2 in the SI).

3. Results and discussion

3.1. X-ray diffraction

X-ray diffraction patterns of Ca_2FeCoO_5 at selected pressures and ambient temperature are shown in Fig. 2. The main detected phase corresponds to solid brownmillerite Ca_2FeCoO_5, with additional peaks arising from a small amount of cobalt oxide impurity and from the gasket material of the high-pressure cell. However, its negligible amount of cobalt oxide (less than 3%) does not significantly affect the pressure dependence of the structural parameters of the main phase (see Fig. S3 of the SI). It should be noted that the crystal symmetry of complex compounds such as Ca_2FeCoO_5 is dependent on the characteristics of the local atomic arrangement,[19,32,33] which can vary depending on the synthesis process used. With this in mind, the orthorhombic *Pbcm*,[31,32] $Pn2_1a$,[26,36] and *I2mb*[36] structural models were tested to describe the XRD experimental data. The Rietveld analysis showed that the *Pbcm* model provided a better fit to the experimental data compared to the other models, and was therefore chosen as the preferred structural model for consideration (see Fig. S4 of the SI). At ambient conditions, the unit cell parameters of Ca_2FeCoO_5 are a =

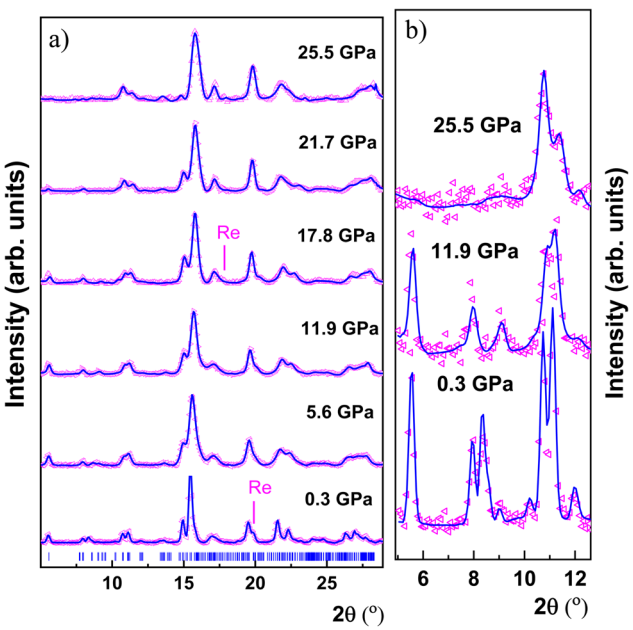

Fig. 2 (a) The X-ray diffraction patterns of Ca_2FeCoO_5 at different pressures and processed using the Rietveld method. Experimental points, calculated profiles, and calculated positions of Bragg reflections for the orthorhombic *Pbcm* phase are shown. Peak (Re) corresponds to high pressure cell material contribution. (b) Enlarged region of the selected XRD diffraction patterns of Ca_2FeCoO_5 at high pressures in the low-angle scattering region. Typical *R*-factor values obtained during the refinement procedure ranged from $R_p = 11.6\%$ and $R_{wp} = 9.7\%$ at 0.3 GPa to $R_p = 8.3\%$ and $R_{wp} = 6.8\%$ at 25.5 GPa.

5.305(8), $b = 11.077(5)$, and $c = 14.642(6)$ Å. These values are comparable to those reported in previous studies.[30–32] Neutron diffraction was initially conducted to determine the atomic coordinates in more detail, as the structure is highly complex and contains numerous atomic positions. In the refinement procedure for the high-pressure X-ray diffraction data, the atomic coordinates were kept fixed to the values obtained from our prior neutron diffraction study, allowing us to reliably calculate lattice parameters, volumes, and distortions without overparameterizing the model. The atomic coordinates obtained from neutron diffraction studies used for processing X-ray data are presented in Table S2, and the obtained structural parameters at various pressures are shown in Table S3. The fact that one of the lattice parameters is doubled in this compound makes it rare among brownmillerite compounds, which have a supercell that is twice the size of the regular brownmillerite unit cell.

At pressures above 6.8 GPa, a gradual disappearance of the weak diffraction peak (110) at $2\theta \sim 8°$ was observed, as well as some broadening of the diffraction peaks in 2θ region of 5–12° were observed. These signs may indicate the occurrence of a structural transition in Ca_2FeCoO_5, leading to an increase in lattice symmetry. However, the possible *I2mb*[32] model was not successful in describing XRD experimental data, so we continued our work using the *Pbcm* structural model and investigated the compressibility of unit cell parameters and volume. The orthorhombic structural model provides a possibility for studying the structural arrangement of ions in the complex brownmillerite structure with superstructures, which allows us to better understand the observed phase transition structural mechanism. However, determining the symmetry of the pressure-induced phase of cation disordered brownmillerite Ca_2FeCoO_5 based on powder X-ray diffraction data remains a challenging task. To accomplish this, single-crystal neutron diffraction is necessary.

The pressure dependencies of the lattice parameters for the brownmillerite Ca_2FeCoO_5 compound are shown in Fig. 3a. The crystal structure of the brownmillerite phase of Ca_2FeCoO_5 can be represented as $a_p\sqrt{2} \times 2a_p\sqrt{2} \times 4a_p$ superstructure, where a_p – lattice parameter of the ideal cubic perovskite unit. For clarity, we have reduced the structural data of Ca_2FeCoO_5 to a distorted perovskite unit representation.

The small anisotropy of lattice parameters compression was observed (Fig. 3a). The calculated average lattice compressibility ($k_{a_i} = -(1/a_{i0})(\mathrm{d}a_i/\mathrm{d}P)|_T$, $a_i = a, b, c$) are $k_a = 0.0013(2)$, $k_b = 0.0017(2)$ and $k_c = 0.0012(1)$ GPa^{-1}. The lattice compression is anisotropic, with the most compressible axis being the *b*-axis. Interestingly, there is a sharp change in the compressibility k_b at pressures around 6 GPa. The compressibility of parameter *b* changes to $k_b = 0.0009(2)$ at high pressures. Uniaxial compression anisotropy can be described by the distortion parameter s_t. This parameter can be defined as $2b/(a + c)$. Fig. 3b demonstrates that the parameter s_t changes its pressure behavior above ~6 GPa. There is a notable change in the slope

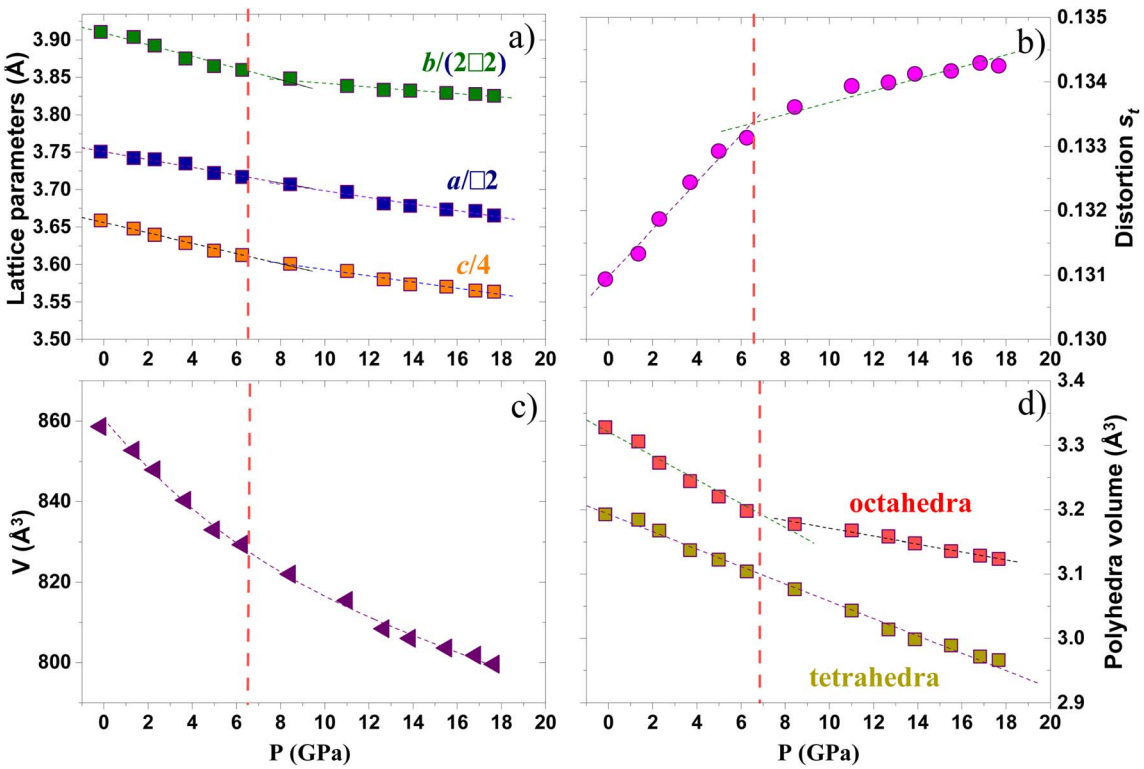

Fig. 3 (a) The reduced to perovskite unit cell lattice parameters of Ca_2FeCoO_5 as functions of pressure and their linear interpolations. (b) The pressure dependence of distortion parameter s_t. (c) The unit cell volume of Ca_2FeCoO_5 as functions of pressure and their interpolations using the Birch–Murnaghan equation of state (1). (d) Pressure evolutions of the volume of octahedra and tetrahedra oxygen units in Ca_2FeCoO_5. Solid lines represent a linear fit of the experimental data. The red dotted line marks a possible phase transition pressure in Ca_2FeCoO_5 compound.

of the pressure dependence of s_t near the phase transition region.

The unit cell volume compressibility data (Fig. 3c) were fitted by the third-order Birch–Murnaghan equation of state:[48]

$$P = \frac{3}{2}B_0\left(x^{-\frac{7}{3}} - x^{-\frac{5}{3}}\right)\left[1 + \frac{3}{4}\left(B' - 4\right)\left(x^{-\frac{2}{3}} - 1\right)\right], \quad (1)$$

where $x = V/V_0$ is the relative volume change, V_0 is the unit cell volume at $P = 0$, and B_0, B' are the bulk modulus ($B_0 = -V(\mathrm{d}P/\mathrm{d}V)_T$) and its pressure derivative ($B' = (\mathrm{d}B_0/\mathrm{d}P)_T$). The fitted values $B_0 = 142(2)$ GPa, $B' = 6.3(5)$, $V_0 = 860.6(4)$ Å^3 for the *Pbcm* phase. The differences between the bulk modules of low-pressure and high-pressure phases are insignificant. This may indicate an orientational change in the octahedral and tetrahedral units in the crystal structure of brownmillerite phase of Ca_2FeCoO_5. The values the B_0 bulk modulus are comparable to the values obtained for similar type of compounds $Ca_2Fe_2O_5$ (B_0 = 127 GPa (ref. 36)), $Ca_2Fe_{2-x}Al_xO_5$ ($B_0 = 128(5)$ GPa (ref. 34)).

The formation of a superstructure in the brownmillerite phase of Ca_2FeCoO_5 results in the creation of two sets of octahedral and tetrahedral units.[31,32] A structural model in which Fe mostly occupies the tetrahedral sites and dominant Co occupies the octahedral sites[30,31] provide more satisfactory studies of the trend of changes in interatomic bond lengths at high pressure. Although the ionic radii of Co^{3+} and Fe^{3+} ions in the oxygen octahedral and tetrahedral coordination are very close, and the expected lattice distortion effect is very small.[10,12] From XRD experimental data, we estimated changes in volumes for octahedral and tetrahedral units (Fig. 3d). It can be seen that the pressure dependence of the volume of a tetrahedral oxygen unit is linear, while an anomaly is observed in an octahedral oxygen unit at pressures around 6 GPa. Oxygen vacancies are known to usually dominate in the octahedral unit,[31,49] which determines differences in the behavior of the oxygen unit volumes of these units at high pressures.

It should be noted that the detected structural phase transition in the brownmillerite-type Ca_2FeCoO_5 compound has a gradual character. This may indicate a structural transformation associated with the reorientation of the oxygen octahedral and tetrahedral units in the brownmillerite crystal structure. In addition, the high-pressure studies of the isostructural compound $Ca_2Fe_2O_5$ indicate a structural phase transition to an orthorhombic structure with $Pn2_1a$ space group at higher pressures of ~12 GPa.[34] However, our results show that the phase transition in Ca_2FeCoO_5 occurs at lower pressures. This can be explained by the peculiarities of the sol–gel synthesis process, which involves the presence of large numbers of oxygen vacancies and redistribution of cobalt and iron cations between tetrahedral and octahedral positions.[14,22,26] These factors can lead to a high impact of internal stresses in the crystal structure of Ca_2FeCoO_5 material, resulting in a decrease in the phase transition pressure.

3.2. Raman spectroscopy

The Raman spectra of the Ca_2FeCoO_5 compound at selected pressures are shown in Fig. 4a. According to the factor group analysis for the *Pbcm* space group[34,36] of the brownmillerite phase of Ca_2FeCoO_5, the 48 active Raman vibrational modes are described as: $\Gamma = 13A_g + 11B_{1g} + 13B_{2g} + 11B_{3g}$. However, the observed Raman bands are much less than those predicted

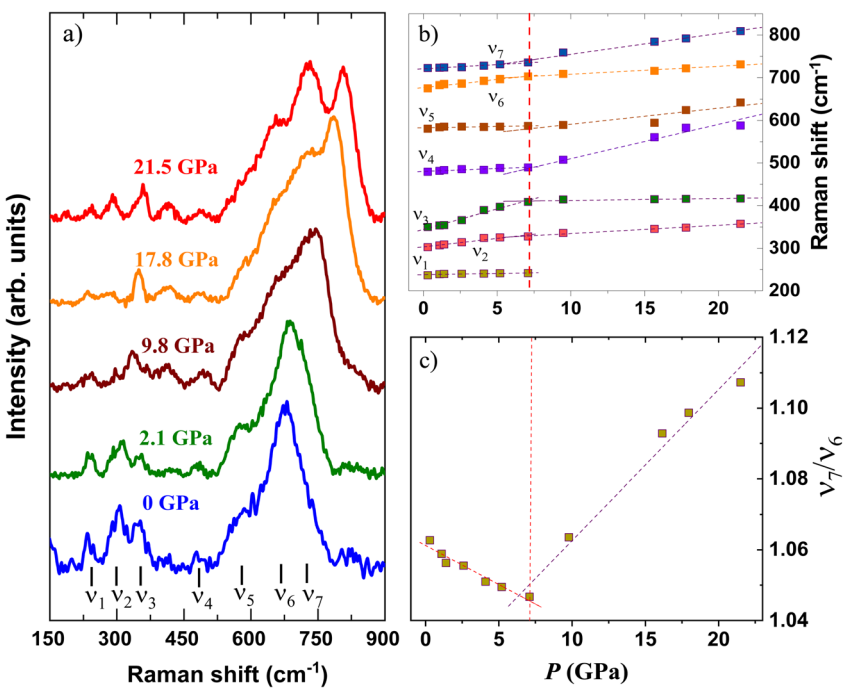

Fig. 4 (a) The Raman spectra of Ca_2FeCoO_5 measured at selected pressures and ambient temperature. The positions of observed modes at ambient pressure are marked. (b) Pressure dependencies of the observed Raman modes. The dotted lines are linear interpolation of experimental data. (c) The relative change of the two vibration lines as a function of pressure.

modes due to some undetected or overlapping vibrations as well as a limited wavenumber range of 200–900 cm^{-1} in the experiment.[34] Seven lines at ~236, ~302, ~349, ~479, ~580, ~675, and ~722 cm^{-1} were detected. These vibrational modes were designated as ν_1, ν_2, ν_3, ν_4, ν_5, ν_6, and ν_7, respectively. The most intense and distinctly resolved bands predominantly correspond to the A_g symmetric modes, as they induce the largest changes in the polarizability tensor.[50–52]

With increasing pressure, an increase in the frequency of all observed vibration modes with different pressure coefficients was detected (Fig. 4b). The calculated pressure coefficients and Grüneisen parameters for the observed vibrational modes are listed in Table S4 of the SI. A representative example of this deconvolution procedure is also presented in Fig. S5 of the SI. Anomalies in the pressure dependence of the Raman modes were observed in the vicinity of the phase transition pressure of $P \sim 6$ GPa. At higher pressures, the Raman line ν_1 at 236 cm^{-1} disappears. According to previous Raman measurements of similar compounds,[25,34,39,52] the lowest frequency bands below ~250 cm^{-1} can be associated with the vibration modes, involving the translational movement of the entire $Fe(Co)O_4$ tetrahedral units.[52] Also the vibration mode ν_3 at 349 cm^{-1} corresponds to the symmetric bending motion of oxygen atoms within the $Fe(Co)O_4$ tetrahedra. There is an anomaly in the pressure behavior of this ν_3 mode. This confirms the proposed model for the phase transition in the $Ca_2Fe_2O_5$ compound, in which the observed pressure-induced transition might relates to the evolution of FeO_4 tetrahedra during compression.

Moreover, the pressure evolution of vibration modes at 479, 675, and 722 cm^{-1} shows fractures in those pressure dependencies. Those modes can be assigned to oxygen motion within octahedral units.[34,36,49] The coexistence of split peaks in the Ca_2FeCoO_5 sample reflects the complexity of the local lattice structure around the octahedral site, due to the heterogeneous distribution of cations Co^{3+} and Fe^{3+}. So, the broad Raman peak in the 500–700 cm^{-1} frequency range is a superposition of the frequencies of stretching vibration of oxygen octahedra. Due to cation distortion in the octahedral position, two types CoO_6 and FeO_6 octahedra units exist in the crystal structure of the Ca_2FeCoO_5 compound.[49] Those octahedra have different compressibilities, and different pressure dependencies of the corresponding vibration frequencies should be observed. In fact, the behavior of the mode changes with pressure during phase transitions (Fig. 4a). If the width of the Raman peak at ~650 cm^{-1} decreases slightly in low-pressure region, then an increase in Raman peak width is observed at pressure above 6 GPa. At higher pressures, a doublet with a shoulder peak is observed (Fig. 4a). We have separated this broad Raman line into two distinct vibrational frequencies, constructing a relative change ν_7/ν_6 in the corresponded frequencies of stretching vibrations of octahedral structures (Fig. 4c). It can be seen that there is a decrease in the splitting of these two modes at low pressures, but a gradual increase in the splitting of ν_7 and ν_6 modes occur as pressure increases above 6 GPa. It is well established that in doped ferrite and manganite systems, the frequencies associated with octahedral stretching vibrations typically manifest as a doublet, corresponding to the distinct vibrational contributions of the host and substitutive dopant ions.[49–52] In the specific case of iron and cobalt, their atomic masses are remarkably similar,[53,54] which results in the corresponding FeO_6 and CoO_6 stretching modes exhibiting closely frequency values. Consequently, monitoring the relative shift of these modes provides a direct probe into the relative pressure-induced variations of the FeO_6 and CoO_6 octahedra. Notably, above 6 GPa, the Grüneisen parameter for the ν_6 mode decreases by a factor of two, while that for the ν_7 mode increases by almost a factor of 2.5 (Table S4). Such a striking divergence in the pressure dependence of these modes indicates a significant change in their relative vibrational behavior. Furthermore, it is known that doped cobalt–iron systems often exhibit local orientational disorder or specific ordering of the corresponding octahedra. Therefore, we propose that the observed anomaly in the pressure behavior of the ν_7/ν_6 ratio, along with the drastic changes in their Grüneisen parameters, reflects a pressure-induced reorientation of the CoO_6 octahedra relative to the FeO_6 octahedra. This structural rearrangement of the cation-oxygen polyhedra is in good agreement with the X-ray diffraction results, which reveal a structural transition in the same pressure range.

It can be assumed that the observed phase transition in brownmillerite-type Ca_2FeCoO_5 is primarily associated with the reorientation and rearrangement of tetrahedral units[49] in the crystal structure. This transformation leads to changes in the corresponding bending and stretching vibration modes of tetrahedral and octahedral oxygen units.[34,36,49] The behavior of these changes indicates an enhanced lattice disorder in the brownmillerite phase of Ca_2FeCoO_5. This is possible due to disordering of iron and cobalt ions in octahedral sites, as well as high rate of oxygen defects in the crystal structure of the brownmillerite phase of Ca_2FeCoO_5.

4. Conclusions

The Ca_2FeCoO_5 compound, possessing a brownmillerite-type structure, was synthesized *via* the sol–gel method. This synthetic approach is characterized by the formation of a defect-rich structure in the resulting compound. Such structural features govern the emergence of a highly distorted phase with the *Pbcm* space group. High-pressure investigations revealed that the synthesized brownmillerite-type Ca_2FeCoO_5 undergoes a phase transition at pressures exceeding 6 GPa. In the vicinity of this transition, anomalies were observed in the pressure dependences of the lattice parameters, as well as in the volumes of the octahedral and tetrahedral units, the degree of octahedral distortion, and the vibrational modes. The detected structural phase transition may be attributed to the reorientation and rearrangement of the tetrahedral units within the crystal lattice, accompanied by an enhanced distortion of the oxygen octahedra.

Author contributions

L. H. Khiem – data curation, project administration, funding acquisition, S. E. Kichanov – writing – original draft, methodology, data curation, conceptualization, funding acquisition, O.

N. Lis – investigation, formal analysis, E. V. Lukin – investigation, methodology, N. T. Nguyen – investigation, formal analysis, N. O. Golosova – investigation, formal analysis, A. G. Asadov – investigation, formal analysis, T. P. Hoang – investigation, formal analysis, Truong-Tho Nguyen – investigation, formal analysis, N. V. Tien – investigation, formal analysis, L. T. P. Thao – investigation, formal analysis, N. T. Dang – writing – review and editing, conceptualization.

Conflicts of interest

There are no conflicts to declare.

Data availability

The data that support the findings of this study are available from the authors upon reasonable request.

Supplementary information (SI) is available. See DOI: https://doi.org/10.1039/d6ra04478f.

Acknowledgements

This work has been supported by the joint grants of the Russian Science Foundation, RSF No. 24-42-04002, https://rscf.ru/project/24-42-04002/ and the grant of the Vietnam Academy of Science and Technology, QTRU06.07/24-26.

References

1 P. Granger, V. I. Parvulescu, S. Kaliaguine and W. Prellier, *Perovskites and related mixed oxides: Concepts and applications*, John Wiley & Sons, 2015.
2 P. Thakur, N. Sharma, D. Pathak, *et al.*, State-of-art review on smart perovskites materials: properties and applications, *Emergent Mater.*, 2024, **7**, 667–694, DOI: 10.1007/s42247-024-00645-w.
3 Y. Tokura, *Colossal Magnetoresistive Oxides*, CRC Press, 2000.
4 C. Chang, W. Chen, Y. Chen, Y. Chen, Y. Chen, F. Ding, C. Fan, H. J. Fan, Z. Fan, C. Gong, Y. Gong, Q. He, X. Hong, S. Hu, W. Hu, W. Huang, Y. Huang, W. Ji, D. Li and Z. Liu, Recent progress on two-dimensional materials, *Acta Phys.-Chim. Sin.*, 2021, **38**(5), 2108017, DOI: 10.3866/pku.whxb202108017.
5 E. Dagotto, T. Hotta and A. Moreo, Colossal magnetoresistant materials: the key role of phase separation, *Phys. Rep.*, 2001, **344**(1–3), 1–153, DOI: 10.1016/s0370-1573(00)00121-6.
6 T. Hotta, M. Moraghebi, A. Feiguin, A. Moreo, S. Yunoki and E. Dagotto, Unveiling new magnetic phases of undoped and doped manganites, *Phys. Rev. Lett.*, 2003, **90**(24), 247203, DOI: 10.1103/physrevlett.90.247203.
7 I. V. Solovyev, Basic aspects of ferroelectricity induced by noncollinear alignment of spins, *Condens. Matter*, 2025, **10**(2), 21, DOI: 10.3390/condmat10020021.
8 L. G. Tejuca and J. L. G. Fierro, *Properties and applications of perovskite-type oxides*, CRC Press, 2000.
9 D. Sedmidubský, V. Jakeš, O. Jankovský, J. Leitner, Z. Sofer and J. Hejtmánek, Phase equilibria in Ca–Co–O system, *J. Solid State Chem.*, 2012, **194**, 199–205, DOI: 10.1016/j.jssc.2012.05.014.
10 L. H. Khiem, O. N. Lis, N. T. Nguyen, S. E. Kichanov, E. V. Lukin, T. N. Vershinina, D. P. Kozlenko, V. T. Nguyen and T. P. Hoang, The crystal and magnetic structure of the $Ca_3Co_2O_6$ manganese-doped compound, *Mod. Phys. Lett. B*, 2026, **40**, 2650025, DOI: 10.1142/S0217984926500259.
11 J. Jin, Y. Wang, C. Zhu, A. Lusi and X. Zhu, Preparation and characterization of $Ca_3Co_2O_6$ as cathode for intermediate temperature solid oxide fuel cells, *Sci. Rep.*, 2016, **187**, 53–55, DOI: 10.1016/j.matlet.2016.10.047.
12 D. P. Kozlenko, N. T. Dang, N. O. Golosova, S. E. Kichanov, E. V. Lukin, P. J. L. Kelley, E. M. Clements, K. V. Glazyrin, S. H. Jabarov, T. L. Phan, B. N. Savenko, H. Srikanth and M. H. Phan, Pressure-induced modifications of the magnetic order in the spin-chain compound $Ca_3Co_2O_6$, *Phys. Rev. B*, 2018, **98**(13), 134435, DOI: 10.1103/physrevb.98.134435.
13 P. Lampen, N. S. Bingham, M. H. Phan, H. Srikanth, H. T. Yi and S. W. Cheong, Macroscopic phase diagram and magnetocaloric study of metamagnetic transitions in the spin chain system $Ca_3Co_2O_6$, *Phys. Rev. B*, 2014, **89**(14), 144414, DOI: 10.1103/physrevb.89.144414.
14 V. Kiryukhin, S. Lee, W. Ratcliff, Q. Huang, H. T. Yi, Y. J. Choi and S. Cheong, Order by static disorder in the Ising chain magnet $Ca_3Co_{2-x}Mn_xO_6$, *Phys. Rev. Lett.*, 2009, **102**(18), 187202, DOI: 10.1103/physrevlett.102.187202.
15 A. Maignan, C. Michel, A. Masset, C. Martin and B. Raveau, Single crystal study of the one-dimensional CaCoO compound: five stable configurations for the Ising triangular lattice, *Eur. Phys. J. B*, 2000, **15**(4), 657–663, DOI: 10.1007/pl00011051.
16 J. Rouxel, M. Tournoux and R. Brec, *Soft chemistry routes to new materials: Chimie Douce*, 1994, pp. 152–153.
17 C. N. R. Rao and K. Biswas, Soft chemistry routes, in *Essentials of inorganic materials synthesis*, John Wiley & Sons, Inc., Hoboken, New Jersey, 2015, DOI: 10.1002/9781118892671.ch10.
18 T. Tran, T. Nguyen, D. Tien, L. Nguyen, T. Hoang, T. Nguyen, L. Son, G. Imanova, S. Jabarov and V. Nguyen, Sol-gel synthesis, characterization and catalytic activity of manganese-doped calcium cobalt oxide, *Next Mater.*, 2025, **8**, 100843, DOI: 10.1016/j.nxmate.2025.100843.
19 K. Mukherjee and E. V. Sampathkumaran, Synthesis of fine particles of a geometrically frustrated spin-chain system, $Ca_3Co_2O_6$, through a pyrophoric route and its magnetic behavior, *J. Alloys Compd.*, 2010, **498**(1), 1–4, DOI: 10.1016/j.jallcom.2010.03.108.
20 F. Ramezanipour, J. E. Greedan, A. P. Grosvenor, J. F. Britten, L. M. D. Cranswick and V. O. Garlea, Intralayer cation ordering in a brownmillerite superstructure: synthesis, crystal, and magnetic structures of Ca_2FeCoO_5, *Chem. Mater.*, 2010, **22**(21), 6008–6020, DOI: 10.1021/cm1023025.
21 G. Sharma, S. Tyagi, V. R. Reddy, A. M. Awasthi, R. J. Choudhary, A. K. Sinha and V. Sathe, Spin-lattice

coupling mediated giant magnetodielectricity across the spin reorientation in Ca_2FeCoO_5, *Phys. Rev. B*, 2019, **99**(2), 024436, DOI: 10.1103/physrevb.99.024436.

22 D. Kowalski, H. Kiuchi, T. Motohashi, Y. Aoki and H. Habazaki, Activation of catalytically active edge-sharing domains in Ca_2FeCoO_5 for oxygen evolution reaction in highly alkaline media, *ACS Appl. Mater. Interfaces*, 2019, **11**(32), 28823–28829, DOI: 10.1021/acsami.9b06854.

23 H. Nakata, A. Ikezawa, T. Okajima and H. Arai, Oxygen evolution reaction activity of highly crystalline hydrated cobalt oxyhydroxide synthesized with soft chemistry, *ECS Meet. Abstr.*, 2024, **MA2024-02**, 3899, DOI: 10.1149/MA2024-02583899mtgabs.

24 E. C. Okpara, O. B. Wojuola, O. E. Fayemi, *et al.*, Sol–gel synthesis and electrochemical sensing properties of brownmillerite calcium ferrite–$Ca_2Fe_2O_5$ nanoparticles, *J. Inorg. Organomet. Polym. Mater.*, 2022, **32**, 3445–3458, DOI: 10.1007/s10904-022-02397-8.

25 E. Tsuji, T. Motohashi, H. Noda, D. Kowalski, Y. Aoki, H. Tanida, J. Niikura, Y. Koyama, M. Mori, H. Arai, T. Ioroi, N. Fujiwara, Y. Uchimoto, Z. Ogumi and H. Habazaki, Brownmillerite-type Ca2FeCoO5 as a practicable oxygen evolution reaction catalyst, *ChemSusChem*, 2017, **10**, 2864, DOI: 10.1002/cssc.201700499.

26 K. Agilandeswari and A. R. Kumar, Optical, electrical properties, characterization and synthesis of $Ca_2Co_2O_5$ by sucrose assisted sol gel combustion method, *Adv. Powder Technol.*, 2014, **25**, 904–909, DOI: 10.1016/j.apt.2014.01.006.

27 J. Zhang, H. Zheng, C. D. Malliakas, J. M. Allred, Y. Ren, Q. Li, T.-H. Han and J. F. Mitchell, Brownmillerite $Ca_2Co_2O_5$: Synthesis, stability, and re-entrant single crystal to single crystal structural transitions, *Chem. Mater.*, 2014, **26**(24), 7172–7182, DOI: 10.48550/arXiv.1411.5615.

28 D. Navas, S. Fuentes, A. Castro-Alvarez and E. Chavez-Angel, Review on sol-gel synthesis of perovskite and oxide nanomaterials, *Gels*, 2021, **7**(4), 275, DOI: 10.3390/gels7040275.

29 E. V. Frolova and M. I. Ivanoskaya, Structural defect formation in inorganic sol-gel derived oxides, *Defect Diffus. Forum*, 2005, **242–244**, 143–158, DOI: 10.4028/www.scientific.net/ddf.242-244.143.

30 E. Tsuji, R. Nanbu, Y. Degami, K. Hirao, T. Watanabe, N. Matsumoto, S. Suganuma and N. Katada, Brownmillerite-type crystalline Ca_2FeCoO_5 ultrasmall particles with single-nanometer dimensions as an active cocatalyst for oxygen photoevolution reaction, *Part. Part. Syst. Charact.*, 2020, **37**(5), 2000053, DOI: 10.1002/ppsc.202000053.

31 A. M. Arevalo-Lopez and J. P. Attfield, Crystal and magnetic structures of the brownmillerite $Ca_2Cr_2O_5$, *Dalton Trans.*, 2015, **44**(23), 10661–10664, DOI: 10.1039/c4dt03780d.

32 H. Krüger and V. Kahlenberg, Incommensurately modulated ordering of tetrahedral chains in $Ca_2Fe_2O_5$ at elevated temperatures, *Acta Crystallogr., Sect. B:Struct. Sci.*, 2005, **61**(6), 656–662, DOI: 10.1107/s0108768105026480.

33 R. Kuwamura, S. Takagi and A. Kyono, Pressure-induced phase transition of oxygen defective perovskite srebrodolskite $Ca_2Fe_2O_5$, *J. Mineral. Petrol. Sci.*, 2023, **118**(1), 230422, DOI: 10.2465/jmps.230422.

34 Z. Li, Y. Yin, J. D. Rumney, S. R. Shieh, J. Xu, D. Fan, W. Liang, S. Yan and S. Zhai, High-pressure in-situ X-ray diffraction and Raman spectroscopy of Ca_2AlFeO_5 brownmillerite, *High Pressure Res.*, 2019, **39**(1), 92–105, DOI: 10.1080/08957959.2019.1571587.

35 Y. Tao, W. Zhang, N. Li, F. Wang and S. Hu, Atomic occupancy mechanism in brownmillerite Ca_2FeAlO_5 from a thermodynamic perspective, *J. Am. Ceram. Soc.*, 2019, **103**(1), 635–644, DOI: 10.1111/jace.16711.

36 S. Zhai, B. Dai, W. Xue, J. D. Rumney, H. Wang, S. R. Shieh and X. Wu, Pressure- and temperature-dependent Raman spectra of $Ca_2Fe_2O_5$ oxygen defect perovskite, *Spectrochim. Acta, Part A*, 2022, **279**, 121436, DOI: 10.1016/j.saa.2022.121436.

37 D. P. Kozlenko, S. E. Kichanov, E. V. Lukin and B. N. Savenko, High-pressure neutron diffraction study of the crystal and magnetic structure of materials at the pulsed reactor IBR-2: Current opportunities and prospects, *Crystallogr. Rep.*, 2021, **66**, 303–313, DOI: 10.1134/S1063774521020073.

38 *Frontiers of high pressure research*, ed. H. D. Hochheimer and R. E. Etters, Elsevier, New York, 2005.

39 D. P. Kozlenko, N. T. Dang, N. O. Golosova, S. E. Kichanov, E. V. Lukin, P. J. Kelley, E. M. Clements, K. V. Glazyrin, S. H. Jabarov, T. L. Phan, B. N. Savenko, H. Srikanth and M. H. Phan, Pressure-induced modifications of the magnetic order in the spin-chain compound $Ca_3Co_2O_6$, *Phys. Rev. B*, 2018, **98**, 134435, DOI: 10.1103/PhysRevB.98.134435.

40 J. F. Moulder, W. F. Stickle, P. E. Sobol and K. D. Bomben, *Handbook of X-ray photoelectron spectroscopy,*, Perkin-Elmer Corporation, Physical Electronics Division, USA, 1992.

41 Q. Xia, X. Liu, J. Zhou, *et al.*, Activation of H_2O_2-HCO_3^- by $Ca_2Co_2O_5$ for pollutant degradation, *Environ. Sci. Pollut. Res.*, 2024, **31**, 48450–48459, DOI: 10.1007/s11356-024-34398-0.

42 M. Vanags, L. Mežule, A. Spule, J. Kostjukovs, K. Šmits, A. Tamm, T. Juhna, S. Vihodceva, T. Käämbre, L. Baumane, D. Začs, G. Vasiliev, M. Turks, I. Mierina, P. C. Sherrell and A. Šutka, Rapid catalytic water disinfection from earth abundant $Ca_2Fe_2O_5$ brownmillerite, *Adv. Sustainable Syst.*, 2021, **5**, 2100130, DOI: 10.1002/adsu.202100130.

43 D. S. Vavilapalli, R. G. Peri, R. K. Sharma, *et al.*, g-C_3N_4/$Ca_2Fe_2O_5$ heterostructures for enhanced photocatalytic degradation of organic effluents under sunlight, *Sci. Rep.*, 2021, **11**, 19639, DOI: 10.1038/s41598-021-99020-6.

44 T. J. Frankcombe and Y. Liu, Interpretation of oxygen 1s X-ray photoelectron spectroscopy of ZnO, *Chem. Mater.*, 2023, **35**(14), 5468–5474, DOI: 10.1021/acs.chemmater.3c00801.

45 H. Idriss, On the wrong assignment of the XPS O1s signal at 531–532 eV attributed to oxygen vacancies in photo- and electro-catalysts for water splitting and other materials applications, *Surf. Sci.*, 2021, **712**, 121894, DOI: 10.1016/j.susc.2021.121894.

46 L. Liu, Y. Bi and J. Xu, Ruby fluorescence pressure scale: Revisited, *Chin. Phys. B*, 2013, **22**(5), 056201, DOI: 10.1088/1674-1056/22/5/056201.

47 J. Rodríguez-Carvajal, Recent advances in magnetic structure determination by neutron powder diffraction, *Phys. B*, 1993, **192**, 55–69, DOI: 10.1016/0921-4526(93)90108-I.

48 F. Birch, Equation of state and thermodynamic parameters of NaCl to 300 kbar in the high-temperature domain, *J. Geophys. Res.*, 1986, **91**(B5), 4949–4954, DOI: 10.1029/jb091ib05p04949.

49 T. Kmječ, N. Nghiem, N. Truong-Tho, D. Kozlenko, S. Kichanov, A. Rutkauskas, V. Nguyen, E. Korneeva, D. Khan, D. H. Giang, T. Phan, D. Bich, G. Rymski, J. Kohout, V. Chlan and N. Dang, Revealing crucial factors governing magnetic properties of high-energy ball-milled $CoFe_2O_4$ nanoparticles, *Ceram. Int.*, 2024, **51**(4), 5168–5180, DOI: 10.1016/j.ceramint.2024.11.491.

50 S. Zhai, B. Dai, W. Xue, J. D. Rumney, H. Wang, S. R. Shieh and X. Wu, Pressure- and temperature-dependent Raman spectra of $Ca_2Fe_2O_5$ oxygen defect perovskite, *Spectrochim. Acta, Part A*, 2022, **279**, 121436, DOI: 10.1016/j.saa.2022.121436.

51 S. Dhankhar, G. Bhalerao, S. Ganesamoorthy, K. Baskar and S. Singh, Growth and comparison of single crystals and polycrystalline brownmillerite $Ca_2Fe_2O_5$, *J. Cryst. Growth*, 2017, **468**, 311–315, DOI: 10.1016/j.jcrysgro.2016.09.051.

52 T.-L. Phan, N. Tran, D. H. Kim, P. T. Tho, B. T. Hui, T. N. Dang, D.-S. Yang and B. Lee, Electronic structure and magnetic properties of Al-doped $Ca_2Fe_2O_5$ brownmillerite compounds, *J. Am. Ceram. Soc.*, 2018, **101**, 2181–2189, DOI: 10.1111/jace.15357.

53 P. Chandramohan, M. P. Srinivasan, S. Velmurugan and S. V. Narasimhan, Cation distribution and particle size effect on Raman spectrum of $CoFe_2O_4$, *J. Solid State Chem.*, 2011, **14**, 89–96, DOI: 10.1016/j.jssc.2010.10.019.

54 D. T. Khan, N. T. Nghiêm, D. P. T. Tien, S. E. Kichanov, T. P. Hoang, A. V. Rutkauskas and Y. I. Aliyev, Crystal structure and vibrational properties of $Ca_3Co_{2-x}Fe_xO_6$ (x = 0.4-1.0), *Adv. Phys. Res.*, 2025, **7**, 48–56, DOI: 10.62476/apr.7148.

